Biomolecule Sensing with Adaptive Plasmonic Nanostructures

Vladimir P. Drachev and Vladimir M. Shalaev

Purdue University, West Lafayette, IN 47907
{vdrachev,shalaev}@purdue.edu

1 Introduction

One of the challenges of biomolecule sensing with surface-enhanced Raman scattering (SERS) is to preserve all of the advantages of Raman spectroscopy applications for structural biology. There are many examples where Raman spectroscopy provides important information on large, macromolecular structures as a whole and in defining small regions of large complexes through ligand–macromolecule recognition (reviewed in [1, 2, 3, 4, 5, 6]). The Raman scattering process involves interplay between atomic positions, electron distribution, and intermolecular forces. Hence, Raman spectroscopy potentially can be one of the techniques used to reveal correlations between structure and function.

It is a common belief that the protein–metal surface interaction may lead to structural changes of proteins and the loss of protein functionality to some extent. To what extent this occurs is a question that needs to be addressed for any particular type of SERS-active substrates. The applicability of SERS to molecular biology has been under extensive study since the 1980s [7]. Despite some unknowns in the SERS process, the molecular mechanisms of biomolecule–metal surface interactions and the distance dependence of the Raman enhancement, SERS has been widely used in biomolecular spectroscopy [8, 9, 10, 11, 12, 13, 14, 15, 16].

In this Chapter we demonstrate several examples of protein sensing with our SERS substrate employing a new, adaptive property of well-known vacuum-evaporated silver films. The deposition of protein solutions on such a film results in the rearrangement of the initial metal nanostructures. Such protein-mediated restructuring leads to the formation of aggregates of metal particles naturally covered and matched with molecules of particular sizes and shapes. This procedure optimizes the SERS signal and, in parallel, stabilizes the metal surface with proteins. Such a substrate, which is referred to as an *adaptive silver film (ASF)*, provides a large SERS enhancement and hence allows protein sensing at monolayer protein surface densities, while enabling the adsorption of proteins without significant changes in their conformational states [17, 18, 19, 20]. For example, we showed that spectral differences in SERS spectra of human insulin and its analog insulin lispro can be detected and assigned to their difference in conformational states. An interesting op-

K. Kneipp, M. Moskovits, H. Kneipp (Eds.): Surface-Enhanced Raman Scattering – Physics and Applications, Topics Appl. Phys. **103**, 351–366 (2006)

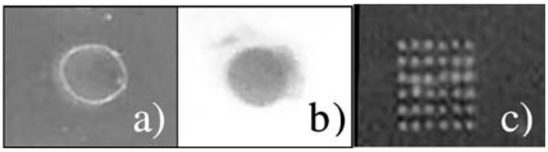

Fig. 1. Typical protein spot on ASF substrate before (**a**) and after (**b**) washing with a Tris-buffered saline solution (the 2 µl aliquot of 0.5 µM bacterial alkaline phosphatase/C-terminal FLAG-peptide fusion (fBAP) was deposited manually), spot size is about 2 mm; (**c**) – antibody array deposited with a quill-type spotter, typical size of about 4 × 4 mm, individual spot size is about 100 µm

portunity is enabled with SERS detection and a pseudotyping procedure for Ebola virus, a potential biowarfare agent. Antibody–antigen binding results in distinct spectral changes in SERS spectra of the first layer protein, either antibody or antigen, depending on the chosen binding scheme. While this Chapter addresses SERS applications, we should mention the excellent performance of adaptive surfaces as a solid support for antibody–antigen binding reactions tested with a microarray protocol and fluorescence detection and compared with commercial substrates [19, 21].

2 Adaptive Plasmonic Nanostructures

Both SERS enhancement mechanisms – electromagnetic and molecular (chemical) – work effectively for molecules in immediate proximity to a rough metal surface. Hence molecule adsorption is an important component of SERS and is always accompanied by surface-chemistry processes. One of the key ideas behind adaptive plasmonic nanostructures is to provide the needed flexibility under protein deposition for surface-chemistry to form particle aggregates naturally covered and stabilized with the proteins of interest.

Figure 1a shows a typical protein spot after manual deposition of proteins in a Tris-buffered saline (TBS) solution on an ASF with subsequent drying. In the example in the figure, the concentration of the deposited antibody was 1 µM and the volume was about 2 µl. After washing with TBS/Tween-20 for 15 min to 30 min, the nonadherent metal is removed from the substrate except in the areas where protein (antibody or antigen) has been deposited (Fig. 1b). An example of an array deposition with a quill-type spotter is shown in Fig. 1c. The capture proteins (a set contains antihuman interleukin 6 monoclonal antibody and other) were dissolved in phosphate-buffered saline (PBS) (300 µg/ml) for spotting on the ASF substrate. The approximate spotting volume was 0.7 nl, yielding spots of about 100 µm in diameter. The substrates were custom printed by Tele-Chem International.

The nanostructures of the ASF before and after protein deposition and washing are shown in Fig. 2a and b. The initial film was fabricated with an e-beam evaporator at high vacuum (10^{-7} Torr); clean glass slides were covered

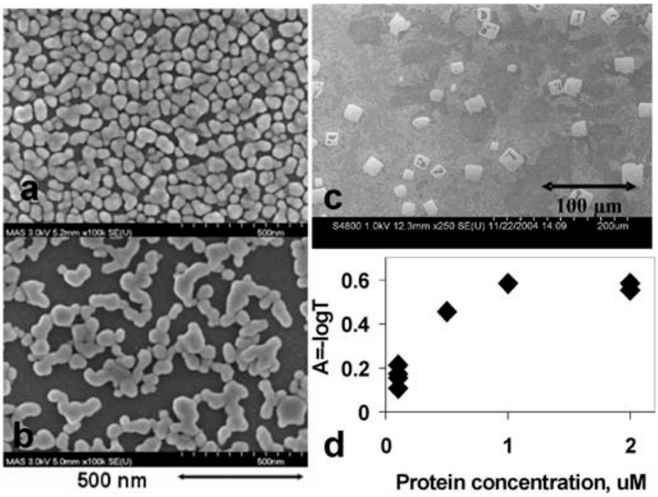

Fig. 2. FE SEM images of ASF substrates: (**a**) initial structure of 11 nm silver film (**b**) same substrate as in (**a**) but inside antibody spot after deposition of 2 µl, 0.5 µM in TBS solution and washing; (**c**) substrate after deposition of TBS without proteins; (**d**) absorbance inside protein spot (antihuman interleukin 10) at 568 nm versus protein concentration. (**a**) and (**b**) are adapted with permission from [19] © 2005 American Chemical Society

first by a sublayer of 10 nm of SiO_2 followed by an 8 nm to 11 nm Ag layer deposited at a rate of 0.05 nm/s. As illustrated by the field emission scanning electron microscope (FE SEM) images, protein-mediated restructuring results in the formation of aggregates of silver particles covered with proteins (Fig. 2b), as opposed to the relatively disintegrated but closely spaced particles of the initial film before protein deposition (Fig. 2a). Depending on the mass thickness of the initial film, small or large fractal-like aggregates can be formed during the nanoscale restructuring process.

A lower concentration of protein results in lower metal coverage (the ratio of white area to total area in the FE SEM images) and lower extinction at a particular wavelength. A decrease of metal coverage correlates with decreasing optical absorption. The absorbance of the metal film inside a protein spot increases linearly with protein concentration and then saturates above a certain concentration, which can be considered to be optimal (Fig. 2d). The concentration dependence shows almost no change after 30 min of washing in TBS/Tween 20 solution, which confirms the stabilization of the film by the proteins.

The transparent areas outside of a typical protein spot certainly contain no silver particles, as indicated by absorption measurements in those areas. The metal-particle coverage inside the protein spot is also reduced relative to the initial film. To determine the chemical form of the silver remaining in the transparent areas, TBS (Tris: 0.05 M, NaCl: 0.138 M, KCl: 0.0027 M) was deposited on the ASF and dried. Then the deposition region was studied with FE SEM and X-ray diffraction analysis. The transparent area contains $40 \times 40\,\mu\text{m}$ particles as seen from FE SEM images (Fig. 2c). X-ray diffraction results indicate a reduced Ag 101 peak and two peaks from NaCl and AgCl. This implies that silver particles are transformed to silver salt in the transparent area.

An estimate of the thermodynamics of the (redox) reaction of Ag with oxygen shows that Ag oxidation is a downhill reaction (with negative free energy) under the experimental conditions. When the silver film is exposed to a TBS buffer (pH 7.4), metal silver tends to be oxidized by oxygen and form AgCl due to the low solubility of AgCl in water ($K_{\mathrm{sp}} = 1.8 \times 10^{-10}$) [22]. The total reaction and its standard potential under standard conditions [22] will be:

$$4\mathrm{Ag} + 4\mathrm{Cl}^- + \mathrm{O}_2 + 4\mathrm{H}^+ = 4\mathrm{AgCl} + 2\mathrm{H}_2\mathrm{O}, \quad E^\circ = E_{\mathrm{ox}}{}^\circ - E_{\mathrm{red}}{}^\circ = 1.007\,\mathrm{V}\,.$$

For calculating the actual reaction potential under the experimental condition at 298 K, we use the Nernst equation:

$$E = E^\circ - (0.059/4)\log\{1/([\mathrm{Cl}^-]^4[\mathrm{H}^+]^4\mathrm{P}_{\mathrm{O}_2}\}\,,$$

where $[\mathrm{Cl}^-]$ is about 0.14 M, $[\mathrm{H}^+]$ is about $10^{-7.4}$ M and the partial pressure of oxygen in air is 0.21 atm. So the experimental value of E is estimated to be 0.51 V, which means that the reaction is thermodynamically favorable (downhill in free energy). The positive potential is the driving force for the oxidation of Ag to Ag^+.

Thus a deposition of proteins in a buffer solution results in the competition of two processes: etching through the oxidation of silver surface in buffer, and stabilization with protein interaction. Etching of the particle surface makes particles movable and leads to the protein-mediated rearrangement of the initial particle nanostructure.

3 SERS Features of Conformational States: Insulin

Insulin represents an interesting example for Raman spectroscopy. It consists of 51 aminoacids distributed in two chains (the A and B chains), which are linked by two disulfide bonds. Insulin typically exists in the hexameric form, although its monomeric form is the active form of the hormone. The size of an insulin hexamer is about 3 nm to 5 nm. The problem of insulin oligomerization has stimulated development of a number of recombinant insulin analogs. The first of these molecules, insulin *lispro,* is engineered as a rapidly acting, blood-glucose-lowering agent. ASFs were used to examine the differences in Raman spectra of two insulin isomers: human insulin and insulin lispro. Both of these molecules have the same set of amino acid side chains, and differ only in the two amino acid residue locations, causing a slight change in the molecules' conformational states. Specifically, the lysine and proline residues on the C-terminal of the B chain are interchanged in their positions in lispro molecules as compared to human insulin. This small difference, however, causes an important clinical effect for diabetes treatment, making insulin lispro a fast-acting agent in the bloodstream while human insulin is slower to act. The differences in SERS spectra between these two insulin isomers can be detected with ASFs and assigned to the α-helix Raman markers and Phe ring-breathing mode.

The Raman system used in this study comprises an Ar/Kr ion laser (Melles Griot), a laser bandpath holographic filter, two Super-Notch Plus filters (Kaiser Optical Systems), focusing and collection lenses, an Acton Research 300i monochromator with a grating of 1200 grooves per millimeter, and a liquid-nitrogen-cooled CCD system (1340 × 400 pixels, Roper Scientific). SERS spectra were typically collected using an excitation laser wavelength of 568.2 nm with normal incidence and 45° scattering. An objective lens (f/1.6) provided a collection area of about 180 μm^2. The spectral resolution was about 3 cm^{-1}. Normal Raman spectra were collected in a backscattering geometry using a micro-Raman system, which consists of a He–Ne laser (632.8 nm) with 12 mW power focused to a spot of about 2 µm diameter on the sample using a 80× microscope objective.

3.1 SERS Versus Normal Raman

A SERS spectrum collected from the central part of an insulin spot is shown in Fig. 3a after linear polynomial background subtraction and normalization. The spot was deposited from a 3 µl drop of 1 µM insulin in a 0.1 mM HCl solution. The extinction coefficient ε_{280} of 5.7 $mM^{-1} \cdot cm^{-1}$ [23] and Raman band assignments are known from the published literature [24, 25].

A comparison of the insulin SERS spectra with our normal Raman spectra of insulin on quartz (Fig. 3b) and with insulin in solution [24] suggests that all the Raman fingerprints of insulin are enhanced by approximately the same factor in our study. Phenylalanine (Phe) and tyrosine (Tyr) often contribute to the protein Raman spectra along with the amide I and amide III bands of the peptide backbone vibrations. Insulin contains phenylalanine located at the B1, B24, B25 residues of the B chain and tyrosine at A14, A19, B16, and B26 [25]. The spectra contain "indicators" of the phenylalanine-to-tyrosine ratio: two peaks at 624 (Phe) and 643 (Tyr) cm^{-1}; the pair of tyrosine Raman makers at 832 and 850 cm^{-1}, the backbone-related C_α–C stretching mode at 945 cm^{-1}; and phenylalanine ring modes at 1003 cm^{-1} and 1030 cm^{-1}. In addition there are a group of peaks between 1150 cm^{-1} and 1500 cm^{-1} that can be constituted from Tyr and Phe peaks at 1176 cm^{-1} and 1206 cm^{-1}, amide III bands at 1242 cm^{-1} and 1267 cm^{-1} (they give the peak at 1248 cm^{-1}, Fig. 3b), –CH deformation modes at 1308 cm^{-1} and 1342 cm^{-1} (peak at 1323 cm^{-1} in our case), a $-COO^-$ symmetrical stretching

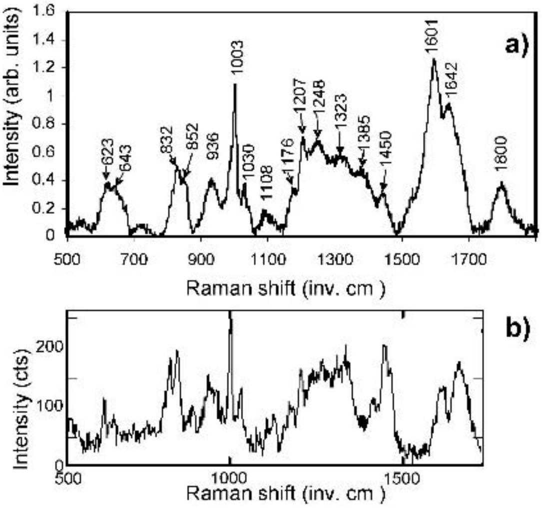

Fig. 3. Recombinant human insulin: (**a**) SERS spectrum after background subtraction and normalization with constant = 7 counts per milliwatt second, (**b**) Raman spectrum of insulin on quartz substrate

mode at 1422 cm^{-1}, and a –CH_2 deformation mode at 1450 cm^{-1}. The spectra also contain overlapped peaks around 1594 cm^{-1} that are usually assigned to the Phe and Tyr modes of an aromatic ring (at 1590 cm^{-1}, 1605 cm^{-1}, and 1615 cm^{-1}), and peaks around 1640 cm^{-1} and higher that are amide I modes of the α-helical (1662 cm^{-1}) and random coil (1680 cm^{-1}) structures [25]. The relative intensities of the Raman peaks are slightly different for SERS of insulin on ASF and for normal Raman of insulin on quartz. The intensity ratios of the Raman peaks (828 cm^{-1} : 850 cm^{-1} : 1003 cm^{-1} : 1450 cm^{-1} : 1600 cm^{-1}) are equal to (0.58 : 0.57 : 1 : 0.32 : 0.35–1.2) for SERS, and (0.54 : 0.64 : 1 : 0.38 : 0.52) for normal Raman on quartz. Note that the 1600 cm^{-1} peak intensity is very sensitive to the experimental conditions; in particular, it grows at high incident light intensity.

The Phe(B1) and Tyr(A14, A19) residues of insulin are exposed to the hexamer surface (Protein Data Bank, `www.pdb.org`), which could be the reason for the similarity between the SERS and normal Raman spectra. It was suggested also in [24] that the Phe peak at 1003 cm^{-1} is mostly composed from one of the three phenylalanine residues, Phe(B1).

The average macroscopic SERS enhancement for insulin on an ASF as measured in our experiments (using the same Raman system for SERS and NR) is about 3×10^6, which is among the largest reported for island or percolation Ag films (10^5 for nitrobenzoate [26] and 5.3×10^5 for *trans*-1,2-bis(4-pyridyl)-ethylene [27]). The enhancement was calculated as an average over the substrate surface probed by the laser beam without normalization on the metal surface coverage, which is about 0.5–0.6 in our case. What is important

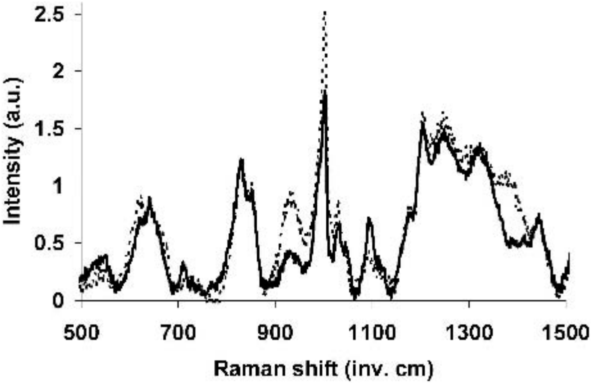

Fig. 4. SERS spectra for human insulin (*dashed gray*) and its analog insulin lispro (*solid black*). Adapted with permission from [17] © 2005 American Chemical Society

for bioapplications is that this enhancement is large enough to detect a submonolayer of proteins, namely 80 fmol/mm^2 surface density for insulin. The protein-mediated aggregation provides a beneficial effect to the sensitivity. It is known that the aggregation of even a few particles makes a large difference for SERS enhancement and can allow single-molecule detection [28, 29, 30].

3.2 Human Insulin Versus Insulin Lispro

Representative SERS spectra for human insulin and insulin lispro are shown in Fig. 4 (dashed and solid lines are human insulin and lispro, respectively, and both spectra were subjected to linear polynomial background subtraction). The spectra were normalized to the Tyr peaks at 832 cm^{-1} and 853 cm^{-1}, since they show approximately equal average intensity over three spots for both human insulin and lispro. Human insulin spectra, as compared to insulin lispro, indicate more intense peaks at 1387 cm^{-1}, 945 cm^{-1}, and for the phenylalanine (Phe) ring-breathing mode at 1003 cm^{-1}. These differences hold at low laser intensity and power (1 mW, laser beam size is about 80 μm to 100 μm) and become less pronounced under exposure to higher laser power.

The zinc–insulin hexamer is an allosteric protein that exhibits two different protein conformations referred to as extended (T) and α-helical (R) conformation states [31]. The T–R state allosteric transitions result in the conversion of B1–B8 residues from a random coil structure to an α-helix conformation along with about 30 Å displacement for the Phe(B1) residue, which can be detected by Raman spectroscopy [24]. Depending on the conformational state of the displaced Phe(B1), the latter can be at different distances and thus have different orientations with respect to the metal surface, enabling the observed increase in Phe peak intensities by a factor of 1.4 for human insulin as compared to insulin lispro.

The C–C_α–H bending band at 1385 cm^{-1} and the N–C–C_α skeletal band at 940 cm^{-1} are stronger in human insulin than in insulin lispro. The 890 cm^{-1} to 945 cm^{-1} band is a characteristic spectral line for an α-helix structure and is known to be sensitive to structural changes [32, 33, 34, 35]. This spectral line is typically centered at 940 cm^{-1} and disappears or displays weak intensity upon conversion to β-sheet or random coil structures. It is also known that the C–C_α–H bending band at 1371 cm^{-1} appears for the R_6 conformation of hexameric human insulin, which has the longest sequence (B1–B19) of α-helix, and disappears in the spectra of $T_3R_3^f$ and T_6 conformations, with (B4–B19) of α-helix for a “frayed” R^f state and (B9–B19) for a T state [32]. Thus the spectral differences in the SERS spectra of the two insulins can be attributed to the larger α-helix content for human insulin and PheB1 displacement. This conclusion is in agreement with X-ray crystallographic studies [36], where it was observed that insulin lispro crystallizes as a $T_3R_3^f$ hexamer. Specific orientations of molecular bonds on the silver surface emphasize the SERS spectral difference between the two insulins, making the differences much stronger than for conventional Raman. Since comparative SERS spectra reveal characteristic features of the insulin and its analog that are correlated with normal Raman and X-ray studies, one can conclude that there is no significant alteration in the conformational states of insulin on the ASFs.

4 Ebola Virus after Pseudotyping

Biological agents are difficult to detect or protect against; they are invisible, odorless, and tasteless, and their dispersal can be accomplished silently. Early detection of a biological agent in the environment allows for early, specific treatment and advanced warning time during which prophylaxis would be effective. Ebola virus is a Class IV biological agent, has a mortality rate up to 90 % and cannot be used safely outside of highly specialized laboratories. The typical size of the Ebola virus is $\sim$ 80 nm to 100 nm in diameter with a shell of about 20 nm; the length can vary from 0.5 µm to 14 µm. The problem of whole-organism detection is the issue of safety, which makes it difficult to test a sensor for such a harmful sample. SERS provides an attractive possibility to detect harmful viruses using the pseudotyping procedure [37]. Through pseudotyping, the shell of the Ebola virus can be attached to the core of a harmless virus [38]. The initial virus loses its capacity to multiply and its activity is completely lost through exposure to UV light. This brings the virus down to a Class I biological agent, which is much easier to handle in typical laboratory environments. At the same time, however, the shell is specific to the given virus and is a glycoprotein that can be detected with SERS since SERS probes the protein layers near the metal surface. Hence

SERS can be considered a label-free whole-organism fingerprinting technique that can be trained with a harmless sample and then be applied to the real, harmful sample.

Our initial studies show spectra of monolayers of the Ebola virus after pseudotyping.[1] Spots of different volumes and different concentrations of the sample were manually deposited on ASF substrates and allowed to dry. SERS spectra were collected from each of the spots on the ASFs and normal Raman spectra were collected from the spots on Teflon-coated ($\sim 15\,\text{nm}$) stainless steel substrates. The SERS substrates were then washed for 5 min with deionized water and dried, after which the spectra were recollected. The background was subtracted from the spectra using a Fourier method. All spectra are normalized. A typical normalization constant is about 10–15 counts per milliwatt second. The SERS spectra of Ebola virus after deposition were obscured by noise-type peaks. The same sample shows good-quality spectra after washing in DI water for 5 min. Washing the substrate after deposition helps by keeping only a monolayer of the virus on the spot, while the extra layers of virus and possible contaminants are washed away. The estimated average surface density for a normal Raman spot is 160 cells per microsquaremeter and that for the SERS spot is 25 cells per microsquaremeter. The normal Raman spectrum was collected from the outer spot ring where the virus density is higher than that of the center, while the SERS spectrum was collected from the center of the spot after washing.

The SERS spectrum of Ebola (Fig. 5a) looks similar to a typical protein spectrum, implying that the outer shell (glycoprotein) signal is enhanced. The normal Raman spectrum (Fig. 5b) is very different since the virus as a whole is probed in this case, including the shell (Ebola) and the core (not Ebola).

5 Tag-Free Antibody–Antigen Binding Detection

The detection of protein–ligand binding events most commonly involves labeling strategies with a variety of schemes, including the use of surface-plasmon resonance (SPR) [39, 40, 41, 42] or surface-enhanced Raman scattering [43, 44, 45]. One of the SERS-based approaches takes advantage of the binding properties of antibody and antigen molecules (or DNA strands) and uses metal nanoparticles coated with Raman-active chromophores as tags [14, 15, 46]. To provide the required level of enhancement, silver clusters are added to form a complex sandwich structure that includes a nanoparticle labeled with a Raman-active dye, complementary biomolecules and the metal clusters. The detection of SERS events without inclusion of exogenous labels has been previously employed for an immune reaction using colloidal

---

[1] The samples were obtained by courtesy of Prof. D. Sanders and Department of Biological Sciences, Purdue University.

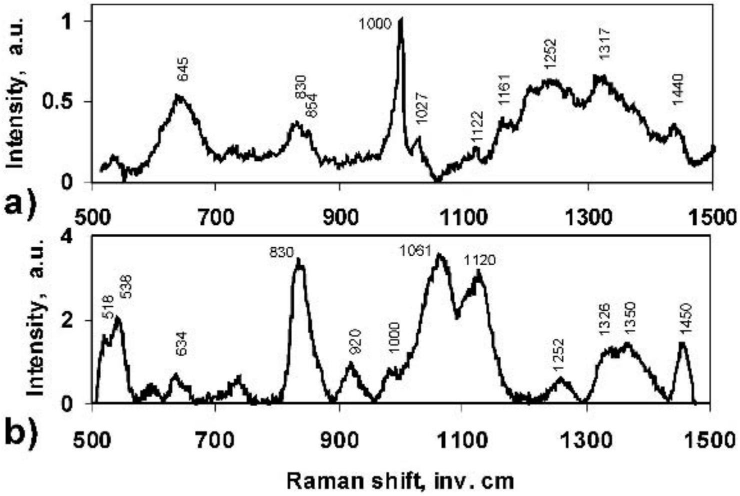

Fig. 5. Spectra of Ebola virus after pseudotyping: (**a**) SERS at $\lambda_{\mathrm{exc}} = 568\,\mathrm{nm}$ and (**b**) normal Raman at $\lambda_{\mathrm{exc}} = 633\,\mathrm{nm}$

gold particles [47]. Other applications of SERS detection for binding to proteins include aflatoxins to RNA polymerase and specific organisms to their respective antibodies [48].

We demonstrated that SERS substrates based on nanostructured adaptive silver films make it possible to detect the formation of specific antigen–antibody complexes at a monolayer level by SERS, fluorescence and chemiluminescence techniques. The antibodies rearrange and stabilize the silver film to make the complex resistant to washing and incubation procedures, while preserving the protein activity as recognition agents. The ASF substrates can potentially be used for routine laboratory analyses in ways similar to membrane-based immunoblotting protocols. One advantage of the ASF substrate is that it does not require chromophore-tagged secondary antibodies since direct detection of SERS spectral signatures associated with the antigen–antibody binding event are observed. These early-stage demonstrations illustrate opportunities for the use of nanoparticle surface systems for analysis of biomolecular interactions relevant for diagnostic applications.

To probe the antigen–antibody binding event using SERS, a general protocol was devised that involves first the deposition and immobilization of a monoclonal antibody or a corresponding antigen on an ASF substrate. Typically, $2\,\mu\mathrm{l}$ of $0.5\,\mu\mathrm{M}$ Ab solution forms a spot of about 2 mm after drying overnight, similar to that shown in Fig. 1. The nonadherent metal particles were then removed by washing with a buffered solution and deionized water to reveal immobilized protein-adapted aggregates representing antibody (or antigen) in a small array. The specific proteins used in our studies include the anti-FLAG M2 monoclonal antibody (fAb) and the bacterial alkaline phosphatase/C-terminal FLAG-peptide fusion (fBAP). Proteins for control experiments included the bacterial alkaline phosphatase (BAP) without the FLAG peptide that was generated by enterokinase cleavage. Subsequent incubation of the protein-adapted aggregates with antigen (or antibody) was conducted, and the nonspecifically bound material was removed by washing with a standard buffer solution for Western blotting (TBS/Tween-20) followed by rinsing five times with deionized water. SERS spectra of the immobilized fAb (or fBAP) were compared before and after reaction with the cognate antigen (or antibody) partner.

An estimated average protein density was about $D_{\text{av}} = 120\,\text{fmol/mm}^2$, or 0.072 molecules per nanosquaremeter. If a single protein molecule occupies an average area of approximately $20\,\text{nm}^2$, then 1.4 layers of protein would be expected in each cluster. This value would represent an upper limit since any loss of protein during the washing steps would reduce the surface coverage; the post-washing surface coverage can be estimated to be monolayer or submonolayer.

The immobilized fAb/metal clusters yielded reproducible SERS results, and representative spectra are shown in Fig. 6a (black). Upon incubation with fBAP (0.75 nM in TBS), spectral changes were observed with the most dominant features appearing in the $1200\,\text{cm}^{-1}$ to $1400\,\text{cm}^{-1}$ region (Fig. 6a, gray). To establish the specificity of the spectral changes, a second array was probed with BAP (0.67 nM) as a control experiment. The spectra of the fAb remained unchanged after incubation with BAP.

In order to further validate our observations regarding the specific interactions on the protein-adapted aggregates, antigen (fBAP at $0.5\,\mu\text{M}$ in TBS) was first deposited on an ASF substrate followed by antibody (fAb at 4 nM) incubation. The results of the SERS measurements are shown in Fig. 6b, and the spectra of fBAP/metal clusters (black trace) undergo changes after incubation with the fAb solution (gray trace). These changes are most evident in the group of peaks centered at $900\,\text{cm}^{-1}$, where a triple peak appears instead of the double peak present before incubation with antibody. The intensity of the peak at $1000\,\text{cm}^{-1}$ is also significantly decreased, while that around $1280\,\text{cm}^{-1}$ is increased.

For both experiments, the signal from the first layer of the protein dominates the SERS spectra observed from the immune complex. Therefore, the spectra shown in Figs. 6a and 6b are significantly different, with the former being primarily the SERS spectrum of the antibody fAb and the latter representing the antigen fBAP spectrum. In both cases, binding with proteins of the second layer results in detectable and reproducible changes in the SERS spectrum of the first layer, revealing strong protein–protein interaction. The fact that the first layer dominates the observed SERS spectra indicates the sharp drop of the enhancement on the scale of several nanometers.

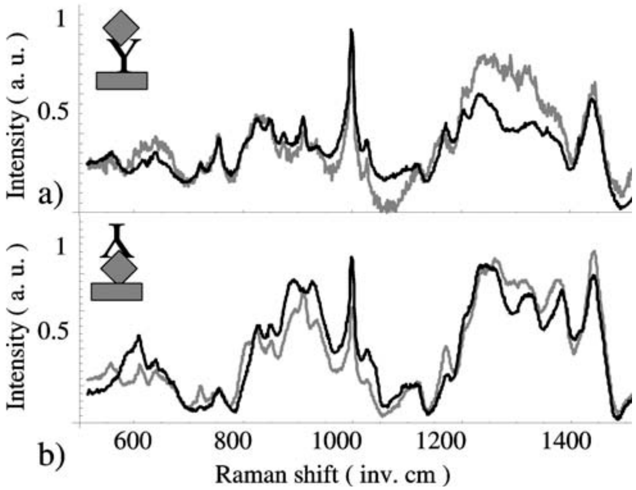

Fig. 6. SERS features of antibody(fAb)–antigen(fBAP) binding reaction on ASF: (**a**) spectra of fAb (*black*), the same fAb-modified surface incubated with fBAP (*gray*), (**b**) inverse order: spectra of fBAP on the ASF substrate (*black*) and the same fBAP-modified surface after incubation with fAb solution (*gray*), $\lambda_{\text{exc}} = 568\,\text{nm}$. Adapted with permission from [19] © 2005 American Chemical Society

6 Protein-Binding Detection with Dye Displacement

SERS spectra of dye molecules and dye conjugate proteins always contain a fluorescence contribution that can be quenched due to the presence of the metal surface, depending on the dye–surface distance. The SERS signal of some molecule placed on the same substrate along with an antibody should be sensitive to the changes in the environment caused by antigen binding, since we detect this signal from roughly a single layer of the molecules. This is the idea of the experiment with rhodamine 6G (R6G) illustrated in Fig. 7.

If we chose a molecule with a high SERS cross section, we have a chance to work with a strong SERS signal while the procedure would be as simple as that of label-free detection described above.

The procedure involves several steps: 1. Manual deposition of 2 µl, 1 µM solution of antihuman interleukin 10 (IL10) in PBS. 2. Incubation of the substrate with 1 nM R6G in TBS Tween 20 for 40 min followed by five DI water rinses. 3. Substrate incubation with 1 nM antigen cocktail containing nine antigens including IL10 in TBS/Tween 20. The antibody concentration was varied from 0.1 µM to 2 µM under deposition from spot to spot. SERS spectra were collected after each step of the procedure shown in Fig. 7 without background subtraction using an excitation wavelength of 568 nm. The spectrum is the antibody, antihuman IL10 spectrum in the first case (Fig. 7a), while the R6G spectrum is observed in the second case (Fig. 7b). After incubation with antigen IL10, the spectrum shows some combination of the decreased

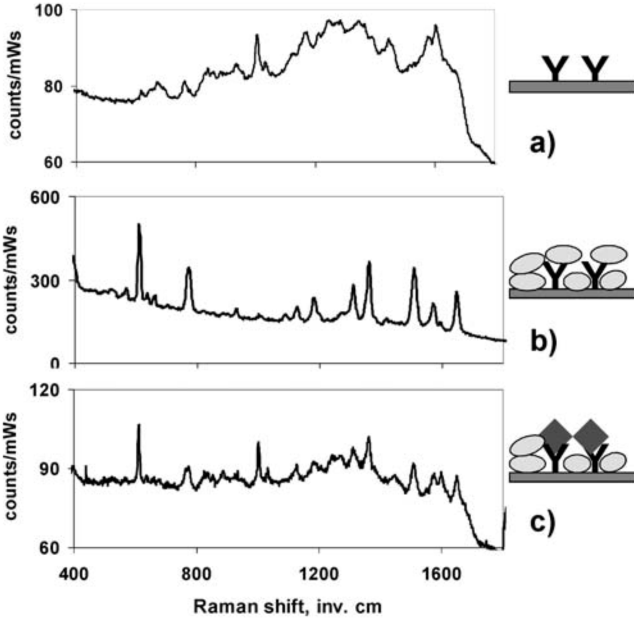

Fig. 7. Sketch of the procedure and corresponding SERS spectra for the experiment on R6G displacement caused by antibody–antigen binding: (**a**) antihuman interleukin 10 manually deposited on ASF (2 µl, 1 µM solution in PBS), (**b**) after incubation with 1 nM R6G in TBS/tween 20 solution (rinsed in DI water 5 times), (**c**) after incubation with antigen cocktail containing 1 nM human interleuikin 10. Spectra are shown without background subtraction

R6G peaks and a slightly modified antibody spectrum. The dependence of the dye signal on the antibody concentration is very different before and after incubation with the antigens providing the binding reaction.

The intensity of the dye SERS signal is highest at the highest concentration (2 µM) initially and becomes highest at the lowest concentration after antigen incubation. The relative change of the R6G signal caused by antigen incubation is approximately inversely proportional to the antibody surface density, as seen in Fig. 8. This suggests a correlation between the displacement of R6G molecules and antigen–antibody binding. The effect of antigen incubation on the displacement of R6G molecules can potentially be applied to binding detection and thus merits further study.

7 Summary

The examples provided demonstrate the appropriateness of nanostructured adaptive silver films (ASFs) to enhance the strength of Raman spectroscopy

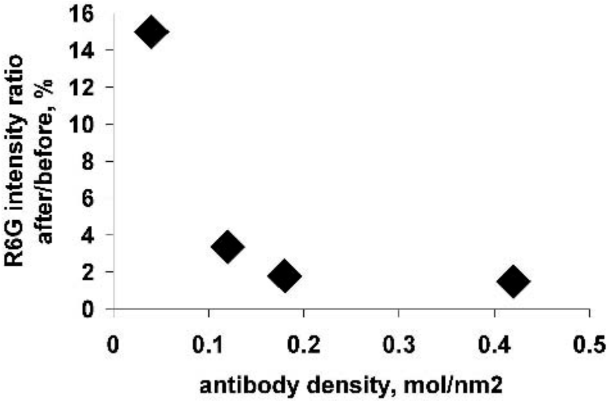

Fig. 8. Intensity of R6G SERS signal (peak at $613\,\text{cm}^{-1}$, background is subtracted) after incubation with antigen solution relative to the intensity before incubation as a function of the average antibody surface density

in biological applications. The restructuring under biomolecule deposition allows one to match the metal-particle aggregate geometry with large molecules such that the conformation and functionality are preserved. This produces excellent conditions for SERS enhancement. Note here that there is a promising way to improve further the sensitivity of SERS-based biosensors by including a bulk metal layer as a sublayer between the adaptive silver film and a glass substrate [20]. The interaction of the silver film with the biomolecule solution acts to stabilize the system, making it applicable for all possible protocols for bioarray treatment and detection. The most straightforward application of SERS in immunoassays appears to be the active signaling reporter for binding reactions. However, we believe the most attractive benefits would be in the direct detection of Raman features of protein–ligand interaction, including a follow-up comprehensive analysis of the vibrational fingerprints.

Acknowledgements

We thank our coauthors M. D. Thoreson, E. N. Khaliullin, V. C. Nashine, H. K. Yuan, Y. Xie, T. Goyani, D. Ben-Amotz, M. L. Narasimhan, and V. J. Davisson who contributed in this work. This work was supported in part by a grant from Inproteo, LLC.

References

[1] T. G. Spiro, B. P. Garber: Ann. Rev. Biochem. **46**, 553–572 (1977)
[2] R. Callender, H. Deng: Ann. Rev. Biophys. Biomol. Struct. **23**, 215 (1994)
[3] W. L. Peticolas: Methods Enzymol. **246**, 389 (1995)

[4] P. R. Carey: J. Raman Spectrosc. **29**, 7 (1998)

[5] R. Callender, H. Deng, R. Gilmanshin: J. Raman Spectrosc. **29**, 15 (1998)

[6] R. Tuma: J. Raman Spectrosc. **36**, 307 (2005)

[7] G. D. Chumanov, R. G. Efremov, I. R. Nabiev: J. Raman Spectrosc. **21**, 43 (1990)

[8] T. Vo-Dinh: Trends Anal. Chem. **17**, 557–582 (1998)

[9] G. Bauer, N. Stich, T. G. M. Schalkhammer: *Methods and Tools in Biosciences and Medicine: Analytical Biotechnology* (Birkhäuser, Basel 2002) pp. 253–278

[10] M. S. Sibbald, G. Chumanov, T. M. Cotton: J. Electroanal. Chem. **438**, 179–185 (1997)

[11] T. Vo-Dinh, D. L. Stokes, G. D. Griffin, M. Volkan, U. J. Kim, M. I. Simon: J. Raman Spectrosc. **30**, 785–793 (1999)

[12] K. R. Brown, A. P. Fox, M. J. Natan: J. Am. Chem. Soc. **118**, 1154–1157 (1996)

[13] K. E. Shafer-Peltier, C. L. Haynes, M. R. Glucksberg, R. P. V. Duyne: J. Am. Chem. Soc. **125**, 588–593 (2003)

[14] Y. W. C. Cao, R. Jin, C. A. Mirkin: Science **297**, 1536–1540 (2002)

[15] Y. C. Cao, R. Jin, J. M. Nam, C. S. Thaxton, C. A. Mirkin: J. Am. Chem. Soc. **125**, 14676–14677 (2003)

[16] D. S. Grubisha, R. J. Lipert, H. Y. Park, J. Driskell, M. D. Porter: Anal. Chem. **75**, 5936–5943 (2003)

[17] V. P. Drachev, M. D. Thoreson, E. N. Khaliullin, V. J. Davisson, V. M. Shalaev: J. Phys. Chem. B **108**, 18046 (2004)

[18] V. P. Drachev, M. D. Thoreson, E. N. Khaliullin, A. K. Sarychev, D. Zhang, D. Ben-Amotz, V. M. Shalaev: Proc. SPIE **5221**, 76 (2003)

[19] V. P. Drachev, V. C. Nashine, M. D. Thoreson, D. Ben-Amotz, V. J. Davisson, V. M. Shalaev: Langmuir **21**, 8368 (2005)

[20] V. P. Drachev, M. D. Thoreson, V. C. Nashine, E. N. Khaliullin, D. Ben-Amotz, V. J. Davisson, V. M. Shalaev: J. Raman Spectrosc. **36**, 648 (2005)

[21] V. P. Drachev, M. L. Narasimhan, H.-K. Yuan, M. D. Thoreson, Y. Xie, V. J. Davisson, V. M. Shalaev: Proc. SPIE **5703**, 13 (2005)

[22] A. J. Bard, R. Parsons, J. Jordan: *Standard Potentials in Aqueous Solution* (Marcel Dekker, New York 1985)

[23] R. R. Porter: Biochem. J. **53**, 320–328 (1953)

[24] D. Ferrari, J. R. Diers, D. F. Bocian, N. C. Kaarsholm, M. F. Dunn: Biopolymers (Biospectroscopy) **62**, 249–260 (2001)

[25] N.-T. Yu, C. S. Lu: J. Am. Chem. Soc. **94**, 3250 (1972)

[26] D. A. Weitz, S. Garoff, T. J. Gramila: Opt. Lett. **7**, 168 (1982)

[27] R. P. V. Duyne, J. C. Hulteen, D. A. Treichel: J. Chem. Phys. **99**, 2101 (1993)

[28] K. Kneipp, Y. Wang, H. Kneipp, L. T. Perelman, I. Itzkan, R. R. Dasari, M. Feld: Phys. Rev. Lett. **78**, 1667–1670 (1997)

[29] S. Nie, S. R. Emory: Science **275**, 1102–1106 (1997)

[30] H. Xu, E. J. Bjerneld, M. Kall, L. Borjesson: Phys. Rev. Lett. **83**, 4357 (1999)

[31] N. C. Kaarsholm, H. C. Ko, M. F. Dunn: Biochemistry **28**, 4427 (1989)

[32] T.-J. Yu, J. L. Lippert, W. L. Peticolas: Biopolymers **12**, 2161–2176 (1973)

[33] M. C. Chen, R. C. Lord, R. Mendelson: Biochem. Biophys. Acta **328**, 252–260 (1973)

[34] B. G. Frushour, J. L. Koenig: Biopolymers **13**, 1809–1819 (1974)

[35] M. C. Chen, R. C. Lord, R. Mendelson: J. Am. Chem. Soc. **96**, 3038–3042 (1976)

[36] E. Ciszak, J. M. Beals, B. H. Frank, J. C. Baker, N. D. Carter, G. D. Smith: Structure **3**, 615–622 (1995)

[37] T. Goyani: MS thesis, School of Electrical and Computer Engineering, Purdue University (2004)

[38] S. A. Jeffers, D. A. Sanders, A. Sanchez: J. Virology **76**, 12463–12472 (2002)

[39] L. A. Lyon, M. D. Musik, M. J. Natan: J. Anal. Chem. **70**, 5177 (1998)

[40] W. Knoll, M. Zizlsperger, T. Liebermann, S. Arnold, A. Badia, M. Liley, D. Piscevic, F. J. Schmitt, J. Spinke: J. Colloid. Surf. A **161**, 115 (2000)

[41] B. P. Nelson, T. E. Grimsrud, M. R. Liles, R. M. Goodman, R. M. Corn: Anal. Chem. **73**, 1 (2001)

[42] J. C. Riboh, A. J. Haes, A. D. MacFarland, C. R. Yonzon, R. P. V. Duyne: J. Phys. Chem. B **107**, 1772 (2003)

[43] T. E. Rorh, T. Cotton, N. Fan, P. J. Tarcha: J. Anal. Biochem. **182**, 388 (1989)

[44] X. Dou, T. Takama, Y. Yamaguchi, H. Yamamoto, Y. Ozaki: Anal. Chem. **69**, 1492 (1997)

[45] J. Ni, R. J. Lipert, G. B. Dawson, M. D. Porter: Anal. Chem. **71**, 4903 (1999)

[46] T. Vo-Dinh, F. Yan, M. B. Wabuyele: J. Raman Spectrosc. **36**, 640 (2005)

[47] X. Dou, Y. Yamguchi, H. Yamamoto, S. Doi, Y. Ozaki: J. Raman Spectrosc. **29**, 739 (1998)

[48] A. E. Grow, L. L. Wood, J. L. Claycomb, P. A. Thomson: J. Microbiol. Methods **53**, 221 (2003)

Index